A search for concentric rings with unusual variance in the 7-year WMAP temperature maps using a fast convolution approach

P. Bielewicz, B. D. Wandelt, A. J. Banday

Monthly Notices
of the
ROYAL ASTRONOMICAL SOCIETY

MNRAS **429,** 1376–1385 (2013) doi:10.1093/mnras/sts424

A search for concentric rings with unusual variance in the 7-year *WMAP* temperature maps using a fast convolution approach

P. Bielewicz,[1,2,3]★ B. D. Wandelt[4,5] and A. J. Banday[1,2]

[1] *Université de Toulouse, UPS-OMP, IRAP, Toulouse, France*
[2] *CNRS, IRAP, 9 Av. colonel Roche, BP 44346, F-31028 Toulouse cedex 4, France*
[3] *SISSA, Astrophysics Sector, Via Bonomea 265, I-34136 Trieste, Italy*
[4] *UPMC Univ Paris 06, Institut d'Astrophysique de Paris, 98 bis boulevard Arago F-75014 Paris, France*
[5] *Department of Astronomy and Physics, University of Illinois at Urbana-Champaign, Urbana, IL 61801, USA*

Accepted 2012 November 15. Received 2012 November 15; in original form 2012 June 7

ABSTRACT

We present a method for the computation of the variance of cosmic microwave background (CMB) temperature maps on azimuthally symmetric patches using a fast convolution approach. As an example of the application of the method, we show results for the search for concentric rings with unusual variance in the 7-year *Wilkinson Microwave Anisotropy Probe* (*WMAP*) data. We re-analyse claims concerning the unusual variance profile of rings centred at two locations on the sky that have recently drawn special attention in the context of the conformal cyclic cosmology scenario proposed by Penrose. We extend this analysis to rings with larger radii and centred on other points of the sky. Using the fast convolution technique enables us to perform this search with higher resolution and a wider range of radii than in previous studies. We show that for one of the two special points rings with radii larger than 10° have systematically lower variance in comparison to the concordance Λ cold dark matter model predictions. However, we show that this deviation is caused by the multipoles up to order $\ell = 7$. Therefore, the deficit of power for concentric rings with larger radii is yet another manifestation of the well-known anomalous CMB distribution on large angular scales. Furthermore, low-variance rings can be easily found centred on other points in the sky. In addition, we show also the results of a search for extremely high-variance rings. As for the low-variance rings, some anomalies seem to be related to the anomalous distribution of the low-order multipoles of the *WMAP* CMB maps. As such our results are not consistent with the conformal cyclic cosmology scenario.

Key words: methods: data analysis – cosmic background radiation – cosmology: observations.

1 INTRODUCTION

A wide range of cosmological projects carried out in the last two decades – observation of supernova, galaxy surveys and measurements of cosmic microwave background (CMB) fluctuations – have resulted in high-quality data enabling the establishment of a standard cosmological model, i.e. the Λ cold dark matter (ΛCDM) model. This model is based on the big bang paradigm formulated in the last century by Alpher, Herman & Gamow (1948) and extended by the inflationary paradigm by Guth (1981). It explains the observed large-scale structure of the Universe as the result of the growth of primordial inhomogeneities in an expanding Universe, generated during an inflationary epoch, and driven by the mechanism of gravitational instability. The rate of expansion and the growth of inhomogeneities depends on the relative amount of the different forms of matter and energy that constitute the total content of the Universe. In the present epoch, the Universe consists of 5 per cent of baryonic matter, 22 per cent of dark matter and 73 per cent of dark energy (Larson et al. 2011). With only a modest number of free parameters, the ΛCDM model is able to successfully fit thousands of observational data points.

However, this model cannot be considered as a fundamental model. It does not explain the nature of dark matter nor dark energy. Furthermore, it postulates the existence of an unknown scalar field responsible for the inflation. Thus, there is a need for stringent tests of the validity of this model by comparison with alternative cosmological theories having different observational predictions.

One example of such an approach is the search in CMB maps for features that are not predicted by an isotropic and homogeneous standard cosmological model. Remarkably, this effort has resulted in several reports of both non-Gaussianity and evidence for the

★ E-mail: pbielew@fuw.edu.pl

breakdown of statistical isotropy in the *Wilkinson Microwave Anisotropy Probe* (*WMAP*) CMB data, as established by many qualitatively different methods. In particular, an intriguing planarity and alignment of the quadrupole and octopole have been demonstrated (Copi, Huterer & Starkman 2004; de Oliveira-Costa et al. 2004; Schwarz et al. 2004; Bielewicz et al. 2005; Land & Magueijo 2005). A localized source of non-Gaussianity, in the form of a very cold spot on the sky of angular scale 10°, has been detected by Vielva et al. (2004) and Cruz et al. (2005). In addition, an asymmetry in large-scale power as measured in the two hemispheres of a reference frame close to that delineated by the ecliptic plane was determined by Eriksen et al. (2004) and Hansen, Banday & Górski (2004) (also Hansen et al. 2009; Hoftuft et al. 2009).

An alternative approach is to search the CMB maps for specific patterns that are signatures of alternative cosmological models. One example of such signatures is the pairs of circles with matching distribution of the CMB anisotropy signal predicted for universes with multiconnected topology (Cornish, Spergel & Starkman 1998). If the size of the fundamental domain were smaller than diameter of the observable Universe, then we should see at least one pair of such matched circles. Such searches, as most recently undertaken by Bielewicz & Banday (2011), have yielded negative results (see also Key et al. 2007). However, as pointed out by Bielewicz, Banday & Górski (2012), with the upcoming Planck data, we should be able to perform a similar search using CMB polarization data as a cross-check of the temperature-based results (see also Riazuelo et al. 2006).

A second example is provided by models of pre-inflationary massive particles (Fialkov, Itzhaki & Kovetz 2010). These predict the existence of concentric cold and hot rings in the CMB and a bulk flow of galaxies towards their centre. The detection of such rings for the *WMAP* maps at 3σ confidence level was reported recently by Kovetz, Ben-David & Itzhaki (2010).

Another example of a model that imprints circular patterns on the CMB sky is due to the theory of eternal inflation (Feeney et al. 2011). Here, collisions of bubble universes leave signatures in the CMB maps with a characteristic profile. Hints of evidence of such signatures in the *WMAP* data were recently reported by Feeney et al. (2011) and McEwen et al. (2012).

Finally, the scenario of conformal cyclic cosmology proposed by Penrose (2009) (see also Penrose 2008, 2010) proposes that the collisions of massive black holes in a previous cycle of the Universe result in a set of concentric rings with low variance on the CMB sky. In this context, rings centred at points with the Galactic coordinates $(l, b) = (105^\circ, 37^\circ)$ and $(l, b) = (252^\circ, -31^\circ)$ have recently merited special attention (Hajian 2011; Moss, Scott & Zibin 2011; Wehus & Eriksen 2011).

In this paper, we perform a complete search for rings with anomalously variances in the *WMAP* CMB maps. For the computation of variance, we use an approach based on fast convolution on the sphere thus enabling the search for concentric rings centred on a high-resolution grid and with radii in the range from 0° to 90°. This significantly extends previous studies that were limited, due to the use of pixel-based methods, to rings centred on a lower resolution grid and radii in the range [0°, 20°]. Furthermore, in addition to the low-variance rings, we search also for the high-variance rings. Though, they are not predicted by the conformal cyclic cosmology scenario, their presence would manifestly contradict the standard inflationary models.

It should be noted that McEwen et al. (2012) used a similar approach in the context of searching for signatures of eternal inflation.

2 DATA

The search for extreme variance rings was performed on the 7-year *WMAP* data (Jarosik et al. 2011). The *WMAP* satellite observes the sky in five frequency bands denoted by *K*, *Ka*, *Q*, *V* and *W*, centred on the frequencies of 22.8, 33.0, 40.7, 60.8 and 93.5 GHz with angular resolutions of approximately 52.8, 39.6, 30.6, 21 and 13.2 arcmin, respectively. The maps[1] are pixelized in the HEALPIX[2] scheme (Górski et al. 2005) with a resolution parameter $N_{\rm side} = 512$, corresponding to 3145 728 pixels with a pixel size of ∼7 arcmin. In particular, we studied the *V* and *W*-band maps corrected for Galactic emission using a template fitting approach (Gold et al. 2011).

3 COMPUTATION OF VARIANCE BY FAST CONVOLUTION ON THE SPHERE

The variance of the CMB in concentric rings with radius r and width Δr centred on pixel i, $\mathrm{Var}_{i,r}(\Delta T)$, can be estimated via the expression

$$\mathrm{Var}_{i,r}(\Delta T) = \frac{\sum_j \Delta T_j^2 M_j B_{ij}^r}{\sum_k M_k B_{ik}^r} - \left(\frac{\sum_j \Delta T_j M_j B_{ij}^r}{\sum_k M_k B_{ik}^r}\right)^2 - \frac{\sum_j \sigma_j^2 M_j B_{ij}^r}{\sum_k M_k B_{ik}^r}, \quad (1)$$

where M_i denotes mask applied to the map and B_{ij}^r is the ring profile such that

$$B_{ij}^r = \begin{cases} 1 & \text{for } r \le \arccos(\hat{\boldsymbol{n}}_i \cdot \hat{\boldsymbol{n}}_j) < r + \Delta r \\ 0 & \text{otherwise} \end{cases}. \quad (2)$$

The sum in the denominators is over the unmasked pixels in a given ring. The last term in equation (1) corresponds to a noise variance term that has to be subtracted to yield an unbiased estimation of the CMB variance. The noise variance in a given pixel σ_i^2 is defined as $\sigma_i^2 \equiv \sigma_{\rm obs}^2 / N_i^{\rm obs}$, where $\sigma_{\rm obs}$ is the rms of noise per observation and $N_i^{\rm obs}$ denotes number of observation of a given pixel. Both of these quantities are provided by the *WMAP* team for each map.

The correction for the noise bias is not needed if we estimate the cross-variance of two differencing assemblies (DAs) for a given band. Such an estimator is not susceptible to uncertainties in the modelling of the noise properties. In this case, the estimator of the variance takes the form

$$\mathrm{Var}_{i,r}(\Delta T) = \frac{\sum_j \Delta T_{1,j} \Delta T_{2,j} M_j B_{ij}^r}{\sum_k M_k B_{ik}^r} - \frac{\left(\sum_j \Delta T_{1,j} M_j B_{ij}^r\right)\left(\sum_j \Delta T_{2,j} M_j B_{ij}^r\right)}{\left(\sum_k M_k B_{ik}^r\right)^2}, \quad (3)$$

where ΔT_1 and ΔT_2 denote maps for two DAs. We will use this estimator to derive most of the results presented below. We checked that the differences between the two estimators are negligible for the 7-year *WMAP* data. In the case of the *W*band, we used co-added maps for two pairs of DAs, i.e. co-added (W1+W2)/2 and (W3+W4)/2 maps.

The computation of the estimator of CMB variance by direct summation over the pixels within the ring for all ring centres is very time consuming. However, one can observe that the variance estimator given by equation (1) is simply the convolution of the square

[1] Available at http://lambda.gsfc.nasa.gov
[2] http://healpix.jpl.nasa.gov

of the masked map, corrected for the mean, with the ring profile of a given radius and width. For the cross-variance, the product of the two maps is convolved with the ring profile. Thus, the computations can be significantly speeded up by use of a technique using fast convolution on the sphere and therefore performing all essential computations in the spherical harmonics space. Because the ring profile is azimuthally symmetric the computations are the same as for convolution with an azimuthally symmetric beam. In order to estimate the variance, we need to perform four such convolutions. We used the fast spherical harmonics transform implemented in the HEALPIX scheme for these computations.

Such an approach allows us to perform a search for rings with an unusual variance centred on a higher resolution grid and for a wider range of ring radii than by using the pixel based methods employed in previous studies. It can be also easily extended to higher moments of the map such as skewness and kurtosis, as well as employed for more general azimuthally symmetric profiles such as discs with an arbitrary radial weighting function. In fact, Bernui & Rebouças (2009, 2010, 2012) and Bernui, Rebouças & Teixeira (2011) have previously computed the skewness and kurtosis of CMB data. However, our approach allows the analysis to be rapidly performed on spherical caps over a range of radii and for all positions on the sky.

Examples of the spherical harmonic window functions for example ring geometries, $b_\ell \equiv B_{\ell 0}/\sqrt{2\ell+1}$, are shown in Fig. 1. Due to the azimuthal symmetry of the ring, the spherical harmonics coefficients,

$$B_{\ell m} \propto \delta_{m0} \int_{\cos(r+\Delta r)}^{\cos(r)} P_\ell(\cos\theta)\, \mathrm{d}\cos\theta, \tag{4}$$

where $P_\ell(\cos\theta)$ are the Legendre polynomials, are non-zero only for modes $m = 0$. The factor $\sqrt{2\ell+1}$ comes from the averaging of the squares of the coefficients over m. The window functions were normalized to one at b_0. Note that, due to pixelization effects, the ring window function corresponding to a pixelized sphere is not exactly equal to the analytical expression for the window function given by relation (4). Moreover, the actual ring profile should vary over the sky due to both the orientation of the ring with respect to the coordinate frame and variation in shape of the HEALPIX pixels. However, this effect is small and its impact on the analysis is negligible. In these computations, we utilize the window functions determined for the set of pixelized rings of given radii and widths centred on the pole.

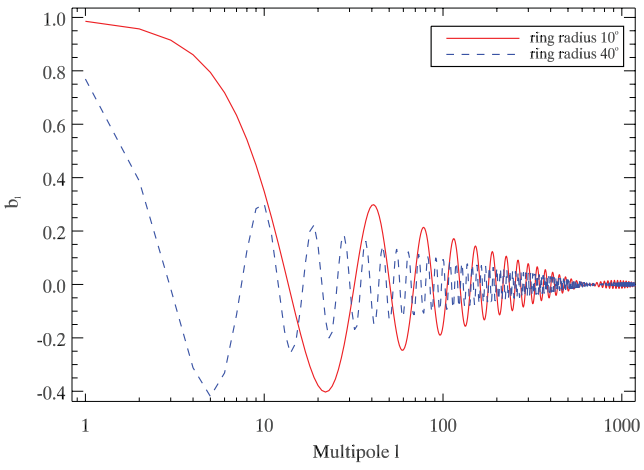

Figure 1. The spherical harmonic coefficients b_ℓ of rings with outer radii of 10° (red solid line) and 40° (dashed blue line) and a width of 0.°5.

As can be seen, the ring window function oscillates around zero with a wavelength $\sim 2\pi/r$ dependent on the ring radius r expressed in radians, i.e. 36 and 9 rad for rings of width 0.°5 with outer radii of 10° or 40°, respectively. Furthermore, because of the $\sqrt{2\ell+1}$ factor in the denominator, the envelope of the widow function falls as $\ell^{-1/2}$. Additional modulation of the envelope depends on the width of the ring Δr. To better understand this behaviour, the ring profile can be considered as a disc of given outer radius from which a smaller disc of the given inner radius is subtracted. The interference of the window functions with slightly different wavelengths corresponding to these discs introduces a modulation with the beat wavelength $\sim 2\pi/\Delta r$. For the ring width of 0.°5, the wavelength is around 720 which corresponds to the node of the window functions seen in the figure. Note also that a larger fraction of the total power for rings with a larger radius comes from the lowest multipoles in comparison to rings with a smaller radius. Thus, the former are more sensitive to the large angular scale power of the CMB maps. This dependence will be clearly seen in the different tests presented in the paper.

Finally, it is worth pointing out that one can consider a more general estimator than that given by equations (1) or (3). The terms in the sum can be weighted with coefficients w_i constrained by additional conditions imposed on the estimator. In the case of an optimal estimator, in the sense of minimization of its variance, the weights are given by $w_i = 1/(S + \sigma_i^2)^2$, where $S \equiv 1/(4\pi)\sum_\ell (2\ell+1)\, C_\ell\, B_\ell^2$ denotes the average CMB variance for the sky observed with an azimuthally symmetric beam characterized by the window function B_ℓ. Nevertheless, for a high signal-to-noise ratio, the variance of the optimal estimator is almost the same as for the suboptimal one. This is the case for the 7-year *WMAP* data. While the CMB variance for the *V*-band map is about 7800 $\mu\mathrm{K}^2$, the median noise variance in a pixel is about 3300 $\mu\mathrm{K}^2$. Indeed, a comparison between the optimal and suboptimal estimator for the *WMAP* data found only negligible differences. Furthermore, the optimal estimator requires additional computing time since two additional convolutions are performed. For these reasons, we decided to use the suboptimal estimator in our analysis.

4 STATISTICS

Here we specify the two statistics used to test the significance of the observed variance profiles – the χ^2 statistic and the number of rings with extreme variance values.

4.1 χ^2 statistic

In order to test the significance of the measured variances for concentric rings centred on a given pixel i, we used the χ^2 statistic defined as

$$\chi_i^2 = \sum_{r,r'} (\mathrm{Var}_{i,r} - \mu_{i,r}) \mathbf{C}^{-1}_{i,rr'} (\mathrm{Var}_{i,r'} - \mu_{i,r'}), \tag{5}$$

where $\mu_{i,r}$ and $\mathbf{C}_{i,rr'}$ are the mean variance and covariance matrix of the variances for a given pixel i, respectively. Note that the application of a mask results in a dependence of the mean and covariance matrix values on the position on the sky of the ring. Consequently, the computation of the χ_i^2 statistic becomes complicated. To store all of the covariance matrices $\mathbf{C}_{i,rr'}$ requires of the order of $N_{\mathrm{pix}} N_{\mathrm{bins}}^2$ bytes of disk space. For maps with N_{pix} pixels on the sky corresponding to a resolution parameter $N_{\mathrm{side}} = 512$, and to a number of bins

$N_{\rm bins} = 180$, corresponding to rings of width 0.°5 with a radius in the range 0°–90°, this corresponds to approximately 400 GB of disk space. Thus, to make these computations feasible, after convolution of the original map with the ring window function in spherical harmonic space, we construct a variance map at $N_{\rm side} = 128$. This is a sufficient resolution to probe the variance distribution in the sky for rings of width 0.°5. Furthermore, we divided the sum over bins of ring radii into three intervals: [0°, 30°[, [30°, 60°[and [60°, 90°[. The required disk space is then reduced to around 2.8 GB.

The conformal cyclic cosmology scenario does not provide well-established predictions for the width of the rings that are being searched for. However, assuming that the typical size is proportional to the ratio of the collision time of the massive black holes to the total time of the previous cycle of the Universe, one can predict that the rings should be very narrow with a width rather below the angular resolution of the *WMAP* maps. Therefore, in this analysis, we only consider rings of width 0.°5, only slightly larger than the angular resolution (∼20 arcmin) of the *V*-band data used predominantly in our analysis. In addition, this choice allows for a straightforward comparison of our results with previous studies. Note that there are also computational constraints on the width of the rings since an analysis with a narrower width is more computationally demanding.

The mean and covariance matrices were estimated on the basis of 1000 Monte Carlo (MC) simulations of the 7-year *WMAP* maps for the standard ΛCDM cosmological model (see Larson et al. 2011, table 3). Another set of simulations allowed the estimation of the significance of the observed values of the χ_i^2 statistic. The χ_i^2 statistic was not computed for any ring for which more than 50 per cent of the component pixels were masked by the *WMAP* KQ75y7 mask. Such rings are delineated by masking the corresponding pixel defining the centre of the ring. Masks for the χ_i^2 maps determined in this way are shown in the figures discussed below.

4.2 Number of extreme variance rings

Another statistic which we used was the number of rings centred on a given pixel with extremely low or high variance. Extreme values were defined to be those deviating from the mean by more than one and a half standard deviations. To estimate the significance of the observed number of extreme rings we use MC simulations of the CMB maps and *p*-values for the null hypothesis, i.e. the probability of getting a larger number of extreme rings for the standard ΛCDM cosmological model. As was the case for the χ^2 statistic, we divided the ring radii into three intervals: [0°, 30°[, [30°, 60°[and [60°, 90°[. If concentric rings of different radii centred at a given point are independent, then the *p*-value for the number of extreme variance rings *n* can be estimated from the cumulative binomial distribution

$$P(n) = \sum_{k>n}^{N_{\rm bins}} \binom{N_{\rm bins}}{k} p^k \, (1-p)^{N_{\rm bins}-k}, \tag{6}$$

where *p* is the probability of getting an extreme variance for a given ring and $N_{\rm bins} = 60$ for one of the three radius intervals of rings with a width of 0.°5. We checked that this approximation of the *p*-value is sufficiently valid for the radius interval [0°, 30°[. However, it is not valid for the other intervals because of strong correlations between rings of larger radii.

5 RESULTS

Before presenting results of the analysis for the full sky, we would like to first address the properties of the sets of concentric rings centred on two points which have recently drawn special attention from the CMB community. This interest was based on claims related to the statistical significance of the variances measured on these rings in the context of the conformal cyclic cosmology scenario proposed by Penrose (2009). The variance profiles for the rings centred at the Galactic coordinates $(l, b) = (105°, 37°)$ and $(l, b) = (252°, -31°)$ for ring radii from 0° to 90° are shown in Fig. 2. Comparing the observed profiles with simulations based on the standard ΛCDM model, we do not identify any significant number of unusually extreme values of the variance in good agreement with the conclusions in Hajian (2011), Moss et al. (2011) and Wehus & Eriksen (2011). However, since our analysis is not limited only to a range of radii from 0° to 20° as in the previous works, we can extend this conclusion to the full range of ring radii from 0° to 90°.

Nevertheless, for the point $(l, b) = (105°, 37°)$, there is evidence of systematically smaller variances for concentric rings with radii greater than 10°. Since such rings are more sensitive to larger angular scales, we consider that the lower variance might be related to the large angular scale anomalies observed in the *WMAP* data, and

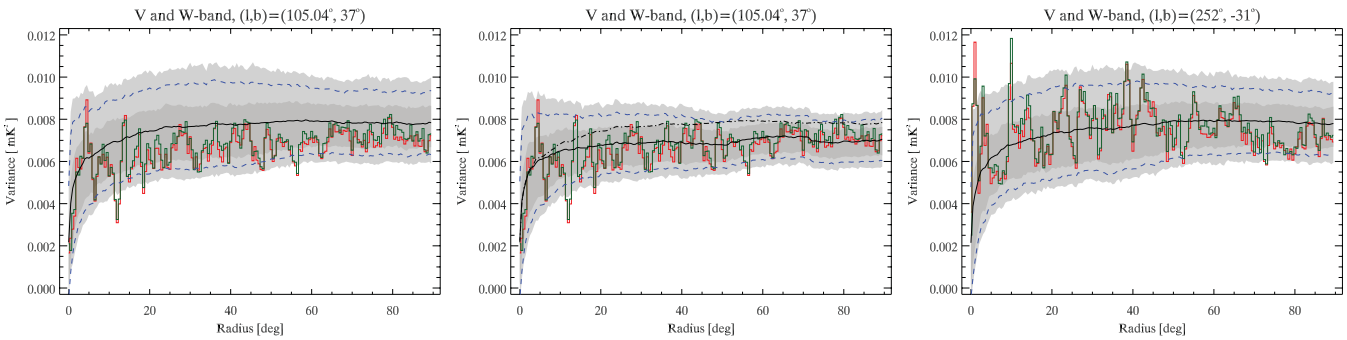

Figure 2. Variance for rings centred at the Galactic coordinates $(l, b) = (105°, 37°)$ (left and middle) and $(l, b) = (252°, -31°)$ (right) with radii in the range [0°, 90°[. The red and green lines denote the variance for the *V* and *W*-band maps, respectively, masked with the KQ75y7 cut. The black lines denote the mean variance estimated from 1000 simulations. The dashed blue lines correspond to the mean shifted up and down by one and a half standard deviations of the variance. The shaded dark and light grey regions indicate the 68 and 95 per cent confidence regions, respectively. In the middle figure, the mean and confidence regions were estimated using simulations with multipoles in the range [0, 7] replaced by the corresponding best-fittting multipoles from the foreground-corrected *V*-band *WMAP* map. The dash–dotted line in this figure denotes the mean for simulations without replacing the lowest order multipoles, i.e. the same mean as in the left figure. Note that the confidence regions are narrower than for the simulations which do not replace the lowest order multipoles. This should not be surprising because the cosmic variance for simulations with fixed best-fitting multipoles must be smaller.

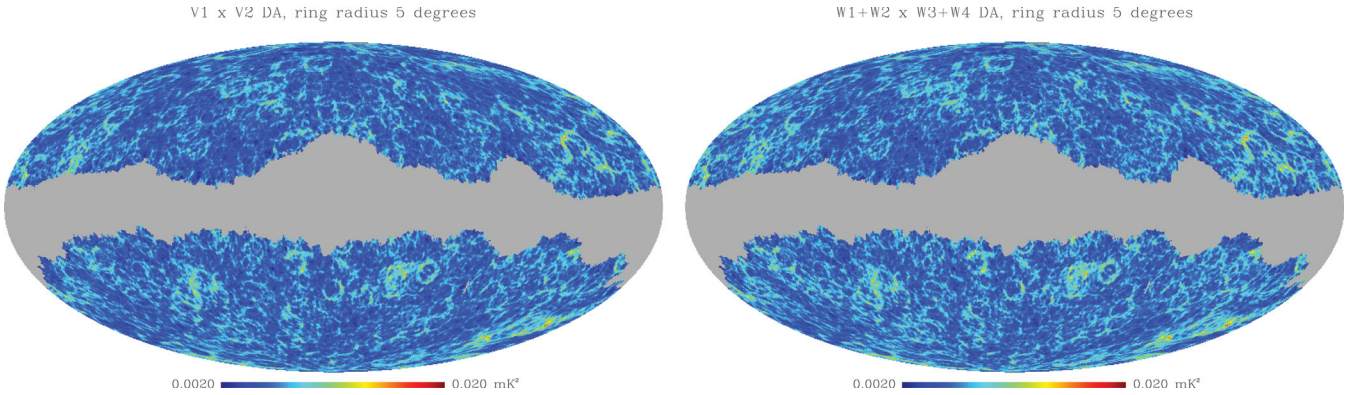

Figure 3. An example of a variance map for rings with a radius of 5°. The left figure shows the variance for the cross-correlation of the V1 and V2 DAs computed after application of the KQ75y7 mask. The right figure shows the analogous map determined from the cross-correlation of two pairs of *W*-band DAs – (W1+W2)/2 and (W3+W4)/2. The grey region corresponds to the pixels for which the variance was not computed due to the mask.

in particular to the hemispherical asymmetry in the power spectrum (Eriksen et al. 2004). Specifically, the point $(l, b) = (105°, 37°)$ lies in the northern ecliptic hemisphere which exhibits less power than the Southern hemisphere. To test this hypothesis, we performed additional simulations in which the lowest multipoles ($\ell \leq 7$) were replaced by the corresponding best-fitting values determined from the foreground-corrected *V*-band data for the KQ75y7 sky coverage.

Specifically, the low-order multipoles were reconstructed from cut sky data using the direct inversion method described in detail in Appendix A. Although this approach is less optimal than the maximum likelihood (de Oliveira-Costa & Tegmark 2006) or Wiener filtering (Tegmark 1997) methods, it provides a reliable and unbiased estimation of the low-order multipoles (Bielewicz, Górski & Banday 2004; Efstathiou 2004). Hereafter, we will refer to the low-order multipoles reconstructed in this way also as the best-fitting multipoles.

Fig. 2 shows that simulations with replaced best-fitting multipoles are more consistent with the data. Replacing fewer multipoles did not reconcile the anomalous behaviour fully, and certainly substituting only the multipoles up to order $\ell = 3$ is not sufficient, suggesting that the large-scale anomalies are not limited only to the apparently aligned quadrupole and octopole.

It is important to note that that a systematically smaller variance for rings with larger radii is not consistent with the conformal cyclic cosmology scenario. In this model, low-variance rings are generated by the collisions of massive black holes in the previous cycle of the Universe. For each of the collisions, one should observe a low-variance ring centred at the position of a given black hole. As the black hole undergoes a series of collisions during its lifetime, we should observe a series of concentric low-variance rings with different radii. Earlier collisions will generate rings with a larger radius while later ones result in rings with a smaller radius. However, for a significant fraction of its lifetime, a black hole will not modify the statistical properties of the CMB sky and rings not related to the collisions will show typical values of the variance. The fact that we find only a few rings with variance bigger than the mean for radii larger than 10° is not consistent with these predictions. As we showed above, the systematically lower variance is much better explained by the anomalous distribution of the low-order multipoles.

In Fig. 3, we show examples of the variance maps for a ring radius of 5°. In appearance, the maps resemble a collection of overlapping rings of different amplitude. The high-amplitude rings are due to pixels with lower or higher values in the original map which also form part of the rings with centres separated by 5°. It is clear that the variance maps are very similar for both *V*- and *W*-band maps. Since we also did not find significant differences between the results for the two bands in the statistics computed below, in the reminder of the paper we show results only for the *V*-band map.

5.1 χ^2 statistic

The χ^2-maps for three radii intervals are shown in Fig. 4. The grey regions correspond to pixels for which the χ^2 statistic was not computed since at least one of the concentric rings centred on a given pixel was masked by more than 50 per cent. It is worth noting that in the case of the intervals [30°, 60°[and [60°, 90°[the χ^2 statistic is computed for those rings centred on some pixels that are located inside the KQ75y7 mask.

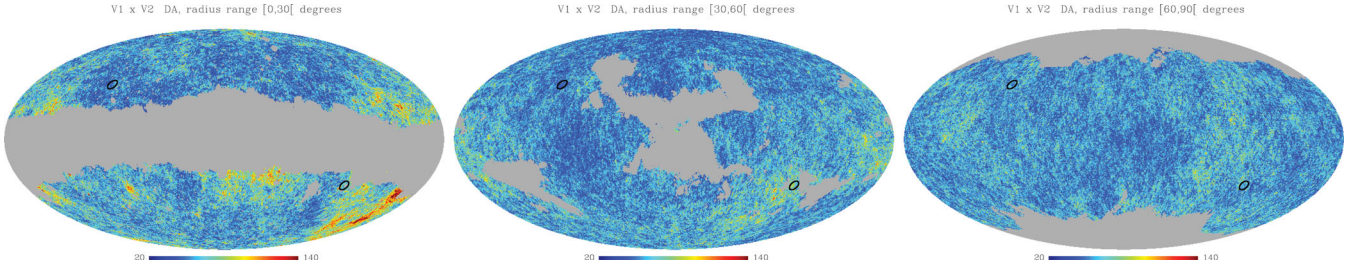

Figure 4. The χ_i^2 map for the three intervals of the ring radii: [0°, 30°[(left-hand column), [30°, 60°[(middle column) and [60°, 90°[(right-hand column). The maps correspond to the cross-correlation of the V1 and V2 DAs masked by the KQ75y7 mask. The black circles are centred at two points analysed in Fig. 2. The grey region corresponds to pixels for which the χ_i^2 was not computed due to the applied mask.

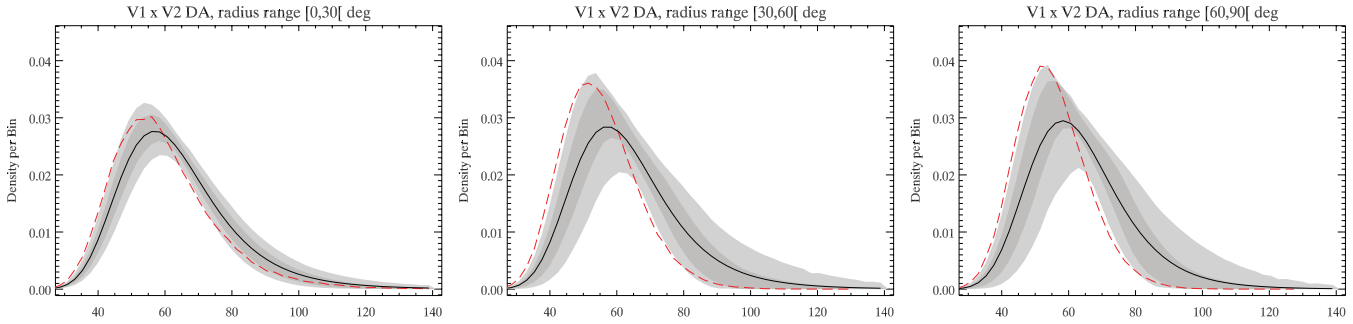

Figure 5. The distribution of the χ_i^2 map for the three intervals of the ring radii: [0°, 30°[(left), [30°, 60°[(middle) and [60°, 90°[(right). The red lines denote the distribution for the *WMAP* maps masked with the KQ75y7 mask and the black lines indicate the mean of the distribution derived from 1000 MC simulations of signal plus noise. The shaded dark and light grey regions indicate the 68 and 95 per cent confidence regions, respectively. The distributions correspond to the cross-correlation of the V1 and V2 DA maps.

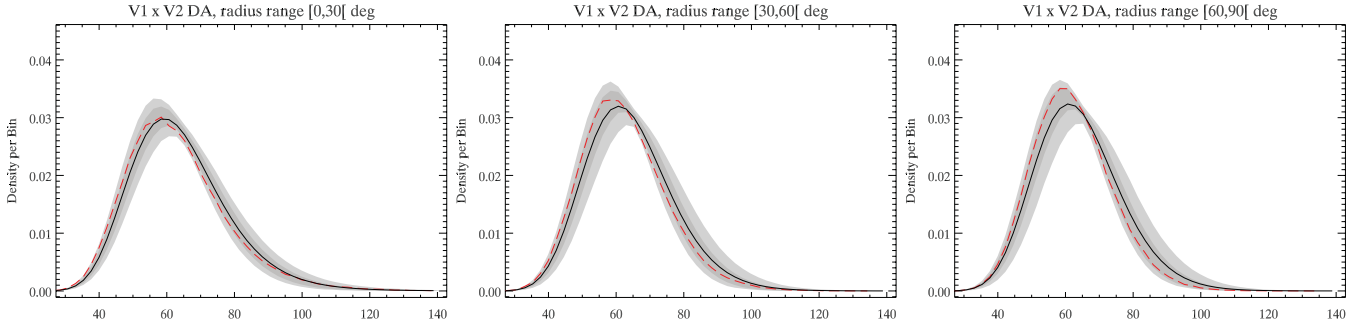

Figure 6. The distribution of the χ_i^2 map after removal of the best-fitting multipoles in the range $\ell \in [0, 7]$ from the V1 and V2 DAs. Plotted lines as in Fig. 5.

There are several regions on the sky with high values of χ^2 for the ring radii in interval [0°, 30°[. However, it is rather unusual that there is a lack of such regions for the χ^2 maps corresponding to rings with radii in the intervals [30°, 60°[and [60°, 90°[.

To test the significance of the features observed in the χ^2 maps, we used 1000 MC simulations of the *WMAP* maps. The distributions of the χ^2 maps are shown in Fig. 5. If the variances for the different rings were uncorrelated, then the number of degrees of freedom would be equal to the number of bins used in computation of the χ^2, i.e. 60 for each of the analysed ring radius intervals. However, due to correlations, the effective number of degrees of freedom will be smaller than 60, and this is apparent from the maximum of the observed distribution. The distribution for the data lies on the border of the 95 per cent confidence region for rings with radii in the intervals [30°, 60°[and [60°, 90°[. For the interval [0°, 30°[, the data are more consistent with the assumed ΛCDM model. Since rings with larger radii are more sensitive to large angular scales, it is plausible that the observed deviation between data and theory is caused by large angular scale anomalies. To test this hypothesis, we repeated the *V*-band analysis for the data from which the best-fitting multipoles in the range $\ell \in [0, 7]$ were removed. Fig. 6 shows that this significantly improves the consistency of the data with the model.

To quantify the difference between the χ^2 distributions recovered from the *WMAP* data and the averaged distribution determined from the MC simulations, we computed the Kolmogorov–Smirnov statistic, with results presented in Table 1. The distance between distributions is significantly smaller after removal of the low-order multipoles.

Correlations in the variance between rings of different radii are shown in Fig. 7. The correlation matrices correspond to rings centred on the Galactic coordinates $(l, b) = (105°, 37°)$ for the three ring radius intervals and are normalized by the diagonal terms of the covariance matrix used in the computation of the χ_i^2 (equation 5). Rings with a larger radius are strongly correlated. This is seen particularly well for the intervals [30°, 60°[and [60°, 90°[. However, removing from the map the best-fitting multipoles in the range $\ell \in [0, 7]$ significantly decorrelates the rings.

Table 1. The Kolmogorov–Smirnov statistic for the cumulative distributions of the χ_i^2 maps presented in Fig. 5 (upper row) and 6 (bottom row).

Radius range	[0°, 30°[	[30°, 60°[	[60°, 90°[
Low-ℓ included	0.110	0.231	0.249
Low-ℓ removed	0.040	0.057	0.065

5.2 Number of extreme variance rings

Fig. 8 shows the probabilities for getting a larger number of extreme rings centred at a given point for the *V*-band maps. Regions with unusually numerous extreme variance rings, such that none of the 5000 MC simulations show a larger number of extreme rings, are denoted by the navy blue colour. The colour range from light blue to red denotes regions with a typical or smaller than typical number of extreme variance rings for the ΛCDM model.

In the case of the interval [0°, 30°[, we can notice that over a large part of the sky, and especially in the northern Galactic hemisphere, the number of rings with extremely high variance is slightly smaller than for most of simulations. However, one can find also regions, mostly in the southern ecliptic hemisphere, where the number of high-variance rings is much larger than for the simulations.

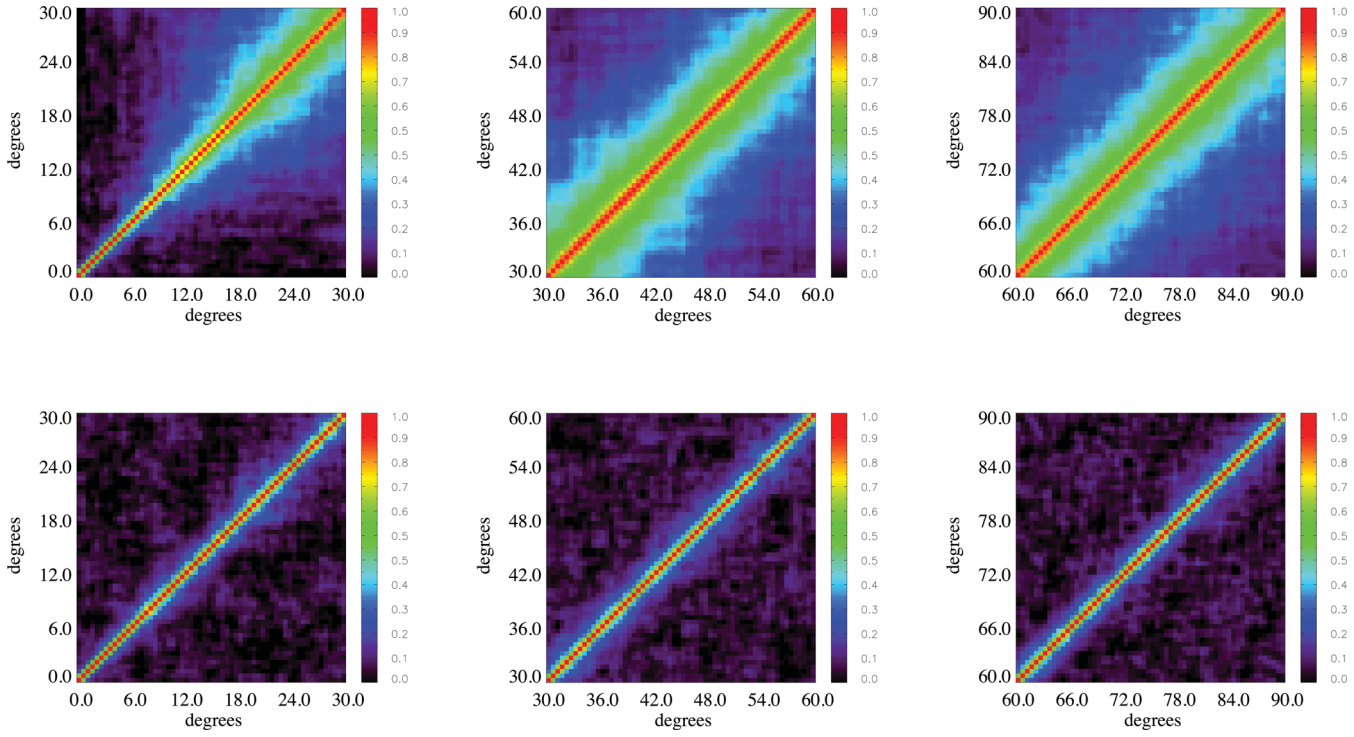

Figure 7. Correlation matrices for the variance on concentric rings centred at the Galactic coordinates $(l, b) = (105^\circ, 37^\circ)$ and ring radius intervals $[0^\circ, 30^\circ[$ (left-hand column), $[30^\circ, 60^\circ[$ (middle column) and $[60^\circ, 90^\circ[$ (right-hand column). The bottom row corresponds to the matrices derived after removing the best-fitting multipoles in the range $\ell \in [0, 7]$ from the maps. The matrices were estimated using 1000 MC simulations.

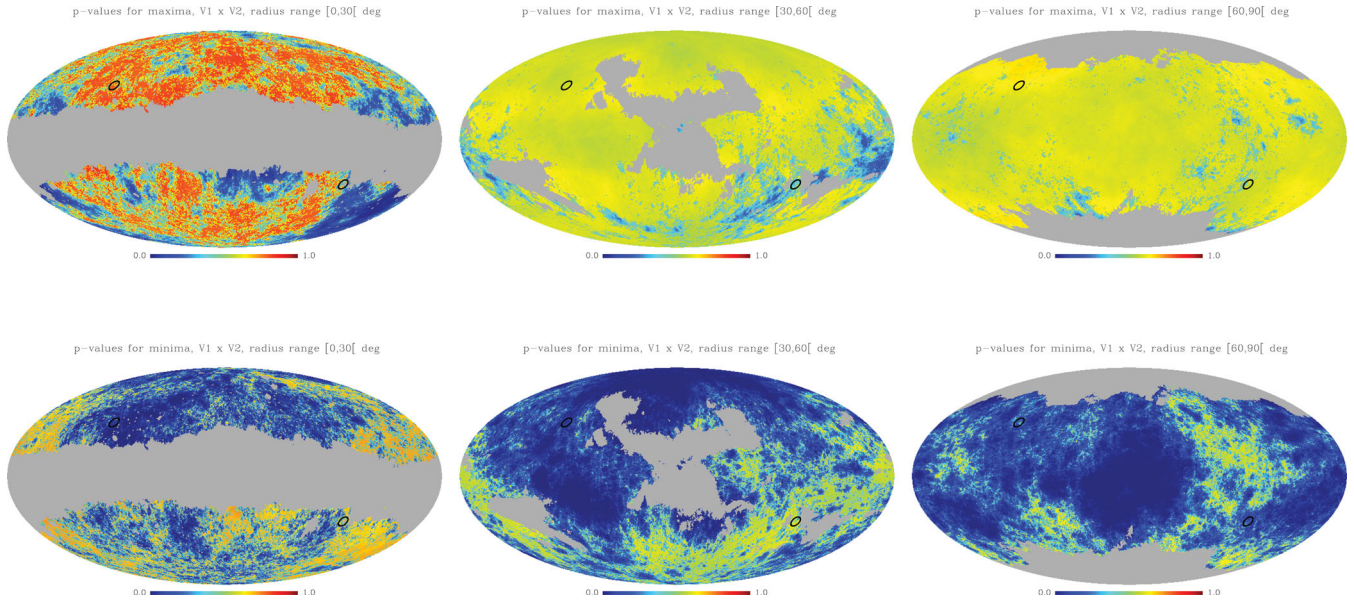

Figure 8. The *p*-values map, estimated from 5000 MC simulations, for rings with extremely high (upper row) and low (lower row) variances for the three intervals of the ring radii: $[0^\circ, 30^\circ[$ (left-hand column), $[30^\circ, 60^\circ[$ (middle column) and $[60^\circ, 90^\circ[$ (right-hand column). The variance map was estimated using the V1 and V2 DAs *WMAP* maps. The black circles are centred at two points analysed in Fig. 2. The grey region corresponds to pixels for which the *p*-values were not computed due to the applied mask.

As one would expect, these regions are clearly anticorrelated with the parts of the sky corresponding to rings with extremely low variance seen in the lower row of the figure, i.e. regions with a higher number of extremely high-variance rings correspond to regions with lower number of extremely low-variance rings and vice versa.

One should notice that the point $(l, b) = (105^\circ, 37^\circ)$, corresponding to the centre of a set of concentric rings with systematically smaller variances, lies in one of the region close to the northern ecliptic pole with many extremely low-variance rings. Any other point in this region shows a similar number of unusually low-variance rings. Such a clustering of rings with low variance is not

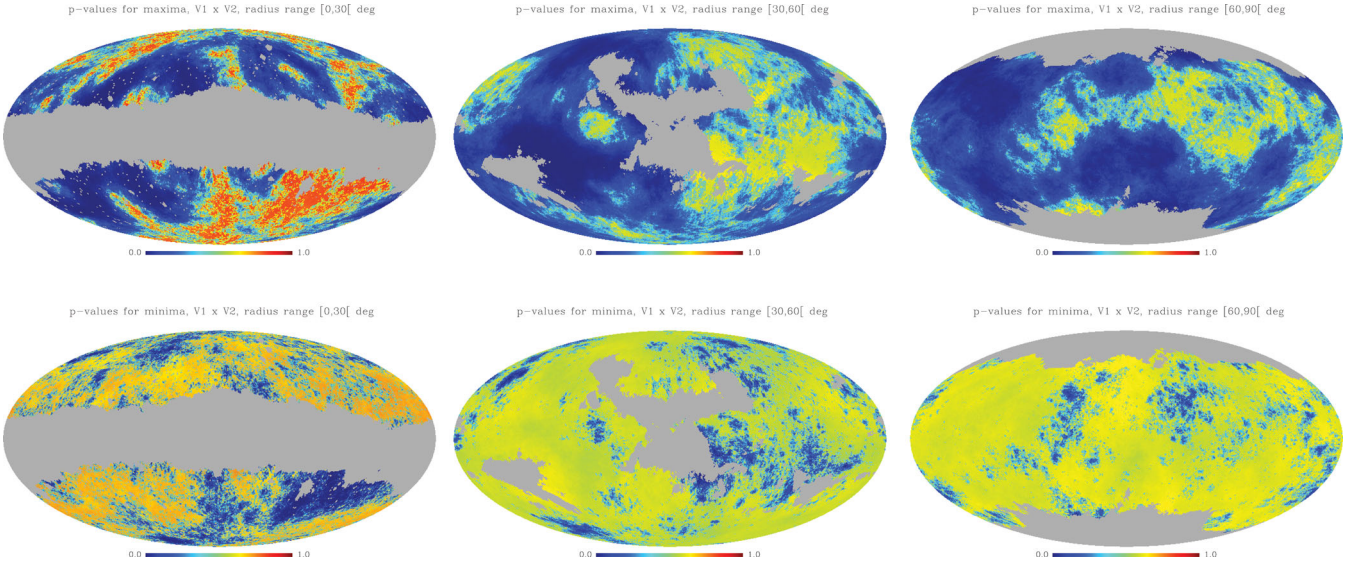

Figure 9. The same as in Fig. 8 but for simulated V1 and V2 DAs.

consistent with the conformal cyclic cosmology scenario. Since the positions corresponding to the massive black holes which generate low-variance rings through collisions are distributed randomly on the sky, the centres of the rings should also be distributed randomly. Clustering of the rings in relatively large regions rather indicates effects related to large angular scale features in the CMB maps.

The anticorrelation between high-variance and low-variance ring regions is seen also for the intervals [30°, 60°[and [60°, 90°[. However, in these cases the p-values for the number of extremely high-variance rings are smaller than for the interval with radii [0°, 30°[. This is a consequence of the stronger correlations between rings of different radii, as the variance for these intervals is more sensitive to the large angular scales. One can also notice fewer regions with small p-values than for the interval [0°, 30°[. Conversely, over a large part of the sky and especially for the interval [30°, 60°[and the northern ecliptic hemisphere, the number of extremely low-variance rings is significantly larger than for simulations. In the case of the interval [60°, 90°[the low-variance rings are centred mostly in the vicinity of the Galactic centre. This disparity in size of regions with extremely high- and low-variance rings is related to the deficit of power at large angular scales in comparison to the best-fitting ΛCDM model.

For comparison, we show in Fig. 9 the p-value maps for simulated V1 and V2 DA maps with the amplitude of the quadrupole close to the average predicted for the concordance ΛCDM model. As we see, contrary to the *WMAP* data, in this case, regions with small p-value are much larger for extremely high-variance rings and much smaller for extremely low-variance rings. This is seen very well for the radius intervals [30°, 60°[and [60°, 90°[. This comparison confirms again the deficit of power of the *WMAP* maps at large angular scales. It also shows that relatively large regions with very small or large probability of getting larger number of extreme rings are generic. Thus, the p-value maps are rather not useful for the estimation of how significant is this deficit. However, they can be used to find parts of the sky with a large number of extreme variance rings that may be interesting for the search for signatures of alternative models of structure formation such as conformal cyclic cosmology.

As for the χ^2 map, we repeated estimation of the p-value maps after removing the best-fitting multipoles in the range $\ell \in [0, 7]$ from both simulations and the V-band DAs. The results are shown in Fig. 10. Since the variance for rings with radii in the interval [0°, 30°[is the least sensitive to the large angular scales, removal of the lowest order multipoles does not significantly change the p-value maps for this interval. The most noticeable change is the reduction of the region of the low-variance rings close to the north ecliptic pole. More significant changes are noticeable for the other two intervals. Since the correlations between rings with different radii after removing of the lowest order multipoles are smaller, the distribution of the p-values looks more similar to the distribution for the interval [0°, 30°[. In the case of the high-variance rings, we can also notice extended regions with lower p-values in the southern Galactic hemisphere. On the other hand, regions corresponding to the extremely low-variance rings are smaller.

Finally, we undertook another test of dependence of the results on the low-order multipoles. We replaced the best-fitting multipoles in the range $\ell \in [0, 7]$ by the same multipoles rotated around the z-axis by 120°. The results for such maps are shown in Fig. 11. After rotation, regions with extremely low-variance rings, especially for the intervals [30°, 60°[and [60°, 90°[, are significantly smaller. However, for the high-variance rings, the changes are less significant. This test would appear to again confirm that, to a large extent, the observed extreme variances of the rings are caused by the lowest order multipoles.

6 CONCLUSIONS

We have presented a fast method for the computation of variance on azimuthally symmetric patches of the sky using a convolution approach. This has enabled the search for a set of concentric rings of width of 0.5 centred at the nodes of a higher resolution grid than would be possible for the pixel-based approach used in previous studies. It has also facilitated the analysis of rings over the full range of radii from 0° to 90°. The technique was applied to the 7-year *WMAP* data to search for rings with unusually low or high variance.

Analysis of the variance of rings centred at two points, $(l, b) = (105°, 37°)$ and $(l, b) = (252°, -31°)$, which have recently drawn special attention in the context of the conformal cyclic cosmology scenario, showed that for the former with ring radius larger

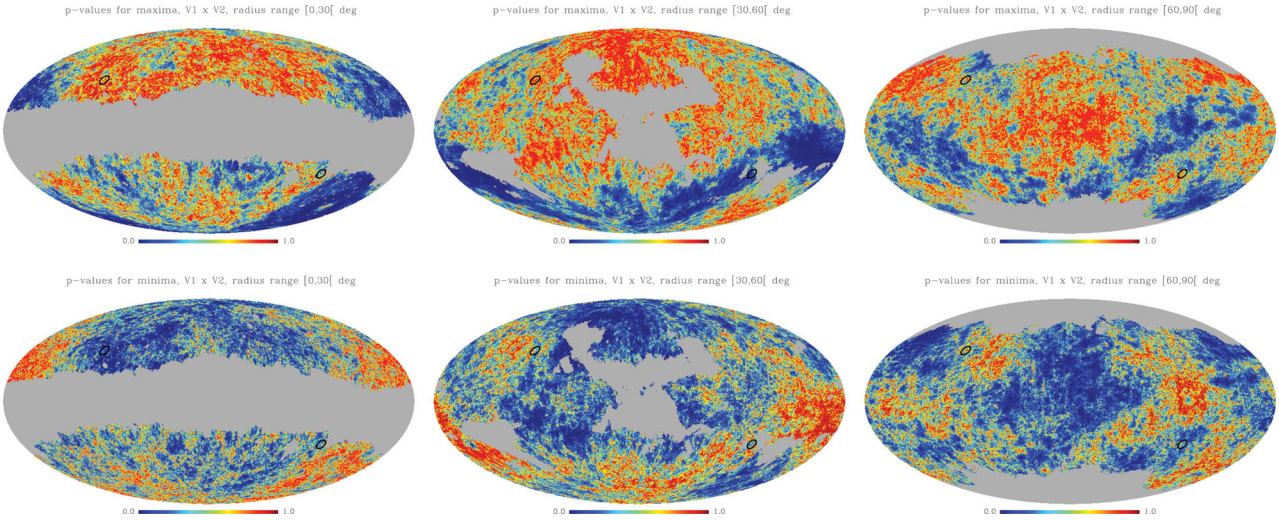

Figure 10. The same as in Fig. 8 but for maps with the best-fitting multipoles in the range $\ell \in [0, 7]$ removed.

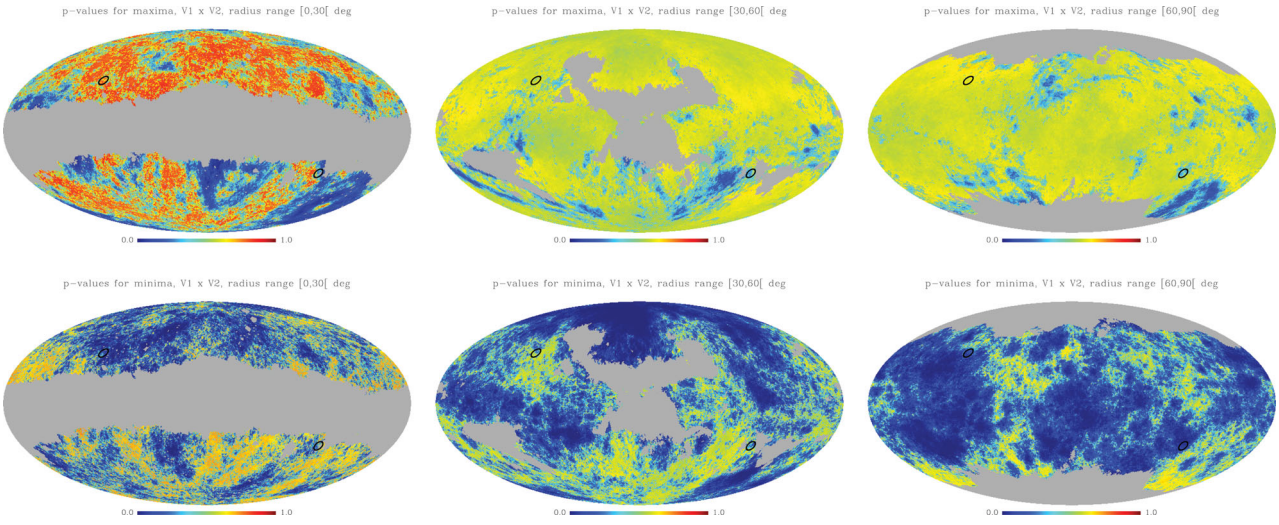

Figure 11. The same as in Fig. 8 but after rotating the best-fittting multipoles in the range $\ell \in [0, 7]$ by 120° around the z-axis.

than about 10° the variance is systematically smaller than the average from MC simulations. However, after replacing the $\ell \in [0, 7]$ multipoles in the simulations with the best-fitting values from the foreground-corrected *V*-band data masked with the KQ75y7 cut, the agreement between simulations and the observed variances is very good. Therefore, we can conclude that the observed deficit of power in rings with large radii is related to the anomalous distribution of the lowest order multipoles of the *WMAP* map. Moreover, the *p*-value maps for the number of extremely low-variance rings show that one can easily find points with as many anomalously low-variance rings as for the point $(l, b) = (105°, 37°)$. Thus, there is nothing unusual in the properties of the rings centred at this point given the observed large-scale anomalies. These results are not consistent with predictions of the conformal cyclic cosmology scenario and they cannot be used to support it. Whilst this model predicts randomly distributed sets of concentric rings within which few have lower variance, we observe sets of rings with systematically lower variance for larger ring radii that are clustered in a few relatively large regions of the sky

A strong dependence of the variance in rings, especially with large radius, on the lowest order multipoles is also seen for other statistics used in our studies. The χ^2 map corresponding to the radius intervals [30°, 60°[and [60°, 90°[takes smaller values than simulations for the best-fitting ΛCDM model at a significance level around 95 per cent. Furthermore, in a large part of the northern ecliptic and Galactic hemispheres, the probability of getting a larger number of extremely low-variance rings is very low, while extremely high-variance regions are much smaller and localized mostly in the southern Ecliptic hemisphere. All of these anomalies disappear after removing from the maps the best-fitting multipoles in the range $\ell \in [0, 7]$. The disparity in distribution of the low- and high-variance rings is also weaker after rotation of the lowest order multipoles around the Galactic poles. Thus, the anomalous variances in rings can be traced to the presence of anomalous low-order multipoles.

However, as we have verified, the removal of the quadrupole and octopole is insufficient to completely eliminate the anomalies. Consequently, we have found that they are also related to higher order multipoles, up to $\ell = 7$. This conclusion is consistent with the results of previous studies on the large angular scale anomalies observed in the *WMAP* data (Hou, Banday & Górski 2009; Hou et al. 2010). Studies of the physical origin of these anomalies are beyond the scope of this paper. However, they do not seem to be

related to residuals of the Galactic thermal dust emission since the results for the *W*-band map are consistent with the results for the *V*-band map.

The fast method of computation of variance presented here can be used for any azimuthally symmetric patches such as discs with an arbitrary radial weighting function. It can also be easily extended to computations of higher order moments enabling various statistical tests of the data on the sphere with high angular resolution. Furthermore, with some performance penalty, the method can be extended to the calculation of moments on non-azimuthally symmetric patches using the more general convolution approach proposed by Wandelt & Górski (2001).

ACKNOWLEDGMENTS

We acknowledge use of CAMB (Lewis, Challinor & Lasenby 2000) and the HEALPIX software (Górski et al. 2005) analysis packages for deriving the results in this paper. We also acknowledge the use of the Legacy Archive for Microwave Background Data Analysis (LAMBDA). Support for LAMBDA is provided by the NASA Office of Space Science.

REFERENCES

Alpher R. A., Herman R., Gamow G. A., 1948, Phys. Rev., 74, 1198
Bernui A., Rebouças M. J., 2009, Phys. Rev. D, 79, 063528
Bernui A., Rebouças M. J., 2010, Phys. Rev. D, 81, 063533
Bernui A., Rebouças M. J., 2012, Phys. Rev. D, 85, 023522
Bernui A., Rebouças M. J., Teixeira A. F. F., 2011, International Journal of Modern Physics: Conference Series, 3, 286
Bielewicz P., Banday A. J., 2011, MNRAS, 412, 2104
Bielewicz P., Górski K. M., Banday A. J., 2004, MNRAS, 355, 1283
Bielewicz P., Eriksen H. K., Banday A. J., Górski K. M., Lilje P. B., 2005, ApJ, 635, 750
Bielewicz P., Banday A. J., Górski K. M., 2012, MNRAS, 421, 1064
Copi C. J., Huterer D., Starkman G. D., 2004, Phys. Rev. D., 70, 043515
Cornish N. J., Spergel D. N., Starkman G. D., 1998, Class. Quantum Gravity, 15, 2657
Cruz M., Martínez-González E., Vielva P., Cayón L., 2005, MNRAS, 356, 29
de Oliveira-Costa A., Tegmark M., 2006, Phys. Rev. D, 74, 023005
de Oliveira-Costa A., Tegmark M., Zaldarriaga M., Hamilton A., 2004, Phys. Rev. D., 69, 063516
Efstathiou G., 2004, MNRAS, 348, 885
Eriksen H. K., Hansen F. K., Banday A. J., Górski K. M., Lilje P. B., 2004, ApJ, 605, 14
Feeney S. M., Johnson M. C., Mortlock D. J., Peiris H. V., 2011, Phys. Rev. D, 84, 043507
Fialkov A., Itzhaki N., Kovetz E. D., 2010, J. Cosmol. Astropart. Phys., 2, 4
Gold B. et al., 2011, ApJS, 192, 15
Górski K. M., Hivon E., Banday A. J., Wandelt B. D., Hansen F. K., Reinecke M., Bartelmann M., 2005, ApJ, 622, 759
Guth A. H., 1981, Phys. Rev. D, 23, 347
Hajian A., 2011, ApJ, 740, 52
Hansen F. K., Banday A. J., Górski K. M., 2004, MNRAS, 354, 641
Hansen F. K., Banday A. J., Górski K. M., Eriksen H. K., Lilje P. B., 2009, ApJ, 704, 1448
Hoftuft J., Eriksen H. K., Banday A. J., Górski K. M., Hansen F. K., Lilje P. B., 2009, ApJ, 699, 985
Hou Z., Banday A. J., Górski K. M., 2009, MNRAS, 396, 1273
Hou Z., Banday A. J., Górski K. M., Groeneboom N. E., Eriksen H. K., 2010, MNRAS, 401, 2379
Jarosik N. et al., 2011, ApJS, 192, 14
Key J. S., Cornish N. J., Spergel D. N., Starkman G. D., 2007, Phys. Rev. D, 75, 084034
Kovetz E. D., Ben-David A., Itzhaki N., 2010, ApJ, 724, 374
Land K., Magueijo J., 2005, MNRAS, 362, 838
Larson D. et al., 2011, ApJS, 192, 16
Lewis A., Challinor A., Lasenby A., 2000, ApJ, 538, 473
McEwen J. D., Feeney S. M., Johnson M. C., Peiris H. V., 2012, Phys. Rev. D., 85, 103502
Moss A., Scott D., Zibin J. P., 2011, J. Cosmol. Astropart. Phys., 4, 33
Penrose R., 2008, in Majid S., ed., On Space and Time, Causality, Quantum Theory and Cosmology, Cambridge Univ. Press, Cambridge, p. 141
Penrose R., 2009, in Tandy C., ed., Death and Anti-Death, Vol. 6: Thirty Years After Kurt Gödel (1906–1978), Ria Univ. Press, Palo Alto, CA, p. 223
Penrose R., 2010, Cycles of Time: An Extraordinary New View of the Universe, Bodley Head, London
Riazuelo A., Caillerie S., Lachièze-Rey M., Lehoucq R., Luminet J.-P., 2006, arXiv:astro-ph/0601433
Schwarz D. J., Starkman G. D., Huterer D., Copi C. J., 2004, Phys. Rev. Lett., 93, 221301
Tegmark M., 1997, ApJ, 480, L87
Vielva P., Martínez-González E., Barreiro R. B., Sanz J. L., Cayón L., 2004, ApJ, 609, 22
Wandelt B. D., Górski K. M., 2001, Phys. Rev. D, 63, 123002
Wehus I. K., Eriksen H. K., 2011, ApJ, 733, L29

APPENDIX A: ESTIMATION OF THE LOW-ORDER MULTIPOLES USING A DIRECT INVERSION METHOD

The low-order multipoles can be reconstructed from the cut sky map using the following relation between the cut sky spherical harmonic coefficients $\widetilde{a}_{\ell m}$ and the full sky coefficients $a_{\ell m}$:

$$\widetilde{a}_{\ell m} = \sum_{\ell' m'} K_{\ell m,\, \ell' m'}\, a_{\ell' m'}, \tag{A1}$$

where

$$\mathbf{K}_{\ell m,\, \ell' m'} \equiv \int_{\text{cut sky}} Y^*_{\ell m}(\hat{\boldsymbol{n}}) Y_{\ell' m'}(\hat{\boldsymbol{n}})\, d\Omega_{\hat{\mathbf{n}}}, \tag{A2}$$

is the spherical harmonics coupling matrix for the cut sky. We assume that noise is negligible for the low-order multipoles, thus it is not included in the above relation.

To estimate the full sky multipole coefficients $\hat{a}_{\ell m}$ one just needs to invert the coupling matrix $\mathbf{K}_{\ell m,\, \ell' m'}$:

$$\hat{a}_{\ell m} = \sum_{\ell' m'} K^{-1}_{\ell m,\, \ell' m'}\, \widetilde{a}_{\ell' m'}. \tag{A3}$$

In general, the sky cut causes the coupling matrix $\mathbf{K}_{\ell m,\, \ell' m'}$ to be singular and it is impossible to reconstruct all of the modes from the $\widetilde{a}_{\ell m}$. However, for low-order multipoles and small sky cuts, a good approximation is to simply truncate the coupling matrix at some multipole ℓ and invert the non-singular truncated matrix.

This estimator provides the full sky $a_{\ell m}$ coefficients that are the best fits to the cut sky map in the sense of minimizing the function

$$\chi^2(a_{\ell'' m''}) = \sum_{\ell m} \left(\widetilde{a}_{\ell m} - \sum_{\ell' m'} K_{\ell m,\, \ell' m'}\, a_{\ell' m'} \right)^2. \tag{A4}$$

It is worth noticing that this method is a straightforward generalization for higher order multipoles of the approach employed in the *remove_dipole* routine from the HEALPIX package. We refer to this method as direct inversion.

This paper has been typeset from a TEX/LATEX file prepared by the author.